RSC Advances

ROYAL SOCIETY OF CHEMISTRY

www.rsc.org/advances

Enhanced electrochemical performance of lead-acid battery by surface modification with multiwall carbon nanotube coating of negative grid

M. Saravanan[†], M. Ganesan, S. Ambalavanan[*]

Electrochemical Energy System Group, CSIR-Central Electrochemical Research Institute, Karaikudi-630006, India

[*] To whom correspondence should be addressed. vananambu456@yahoo.co.in Tel.: +91-4565-224390; Fax: +91-4565-227779

[†] Present address: Flour Milling, Baking & Confectionery Technology Division, CSIR-Central Food Technological Research Institute, Mysore-570020, India

Abstract:

High-performance lead–acid battery (LAB) negative grids have been prepared by a simple carbon nanotube (CNT) coating method. To assess the properties of these materials for use in LAB system, galvanostatic charging – discharging measurement, electrochemical impedance spectroscopy (EIS) and cyclic voltammetry (CV) were performed. The morphology and chemical composition of CNT coating on the negative grid have been investigated by scanning electron microscopy (SEM), Raman spectroscopy and energy dispersive spectrometry (EDS) characterizations. The results clearly demonstrate that CNT coating is uniform, fully covered on the negative grid of LAB, which act as a CNT adhesion layer (CNTAL) between current collector to negative active materials (NAM) and improve the electrical conductivity. Moreover, an enhanced charge acceptance, excellent electrochemical performance and cycling stability have been observed from these CNT coated electrode in comparison to their uncoated electrode. The obtained result reveals that CNT coating not only reduces the charge transfer resistance but also protects NAM from irreversible lead sulfation.

1. Introduction

Lead-acid batteries (LAB) have been highlighted as one of the most promising electrochemical energy storage devices for more than 150 years.[1] Among the various secondary battery systems, LAB is still extensively used in the automotive, power back up system, smart grid and stationary applications.[2] The most important advantages of LAB is operational safety, use of low-cost and high abundant materials, easy construction and well-recognized recycling technology which makes as appealing candidate in the energy storage system.[3] In contrast, Lithium-ion batteries (LIB) power millions of laptop computers, vehicle electrification and other portable electronics applications**,** despite the Li material resource is limited in the earth's crust [4,5] and recycling process is technically elusive due to different type of chemistry used in LIB. At present less than 1% of lithium is recycled and it costs more than five times compared with primary production of Li metal.[6] Interestingly, LAB is more than adequate for many emerging energy storage applications and for a new generation of burgeoning advanced hybrid electric vehicles (HEV) batteries. Unfortunately, the reversibility of lead and lead dioxide active materials still remain a major issue. To overcome such pertinent technical challenges, employing with various carbon - based conductive additives/materials are being under focus.[7-18] To date, all experimental data from world-wide have been indicated the presence of carbonaceous material into the active mass of negative electrode based on the structural affinity between the lead and carbon. [19-22]

In recent years, several reports demonstrated that it is possible to configure carbon - based inter / adhesive layer between current collector to active material and electrode to separator which improves the cyclic performance of the lithium and sodium battery systems.[23-31] An another attractive strategy is to improve the electrical conductivity and performance of supercapacitor, microbial fuel cells, solar cells and LIB electrodes by

impregnating with conductive wrapping,[33] brush-coating,[34] spraying[35] and dipping[36] technique of CNT ink / graphene based materials.[37-40]

Therefore we adapted this approach to our LAB negative electrode and which gives a remarkable cycling performance. The primary function of grids provides an electrical contact between the positive and negative active materials which serves to conduct the current. Additionally, the grid/active material interface play a significant factor that determines the positive active material (PAM) utilization.[41, 42] The very low electronic conductivity of grid/active material interface hampered the PAM within the pellet and leading to increased ohmic drop.[43] These issues can be addressed through numerous approaches for making superior positive electrodes.[44-51] On the other hand, the grid/NAM interface region, which is not discussed in the LAB normal cycling operations and is given minor importance to this region. However, modern society with high rate cycling operation this region (grid resistance) also plays a pivotal role to determine the performance of LAB.[52] Furthermore, this region is not having desirable conductive it will impede the current flow, increases the ohmic drop, non-uniformity of the potential distribution across the grid and promote hydrogen evolution instead of transferring electron to the NAM in high rate cycling.[52,53]

Though NAM consists of a primary (skeleton) / secondary (energetic) structures, these two structures play a most prominent role in negative plate operation. Moreover, the function of energetic structure participates mainly in the processes of current generation and the skeleton structure is the mechanical carrier of the energetic structure and conducts the electric current from the plate grid to every point of the NAM.[54-56] Thus the grid/ skeleton structure interface region might allow high current with very low resistance if the NAM is being fully discharged condition. Many of the earlier studies demonstrated that improving the negative grid conductivity and uniformity of active material utilisation by modification of grid and tab designs.[57, 58] In another approach light weight/conductive grid made from lead

coated graphite, [59] reticulated vitreous carbon (RVC), [60] carbon / graphite foams [61, 62] and polyaniline [63] coated negative electrodes were used. However, the introduction of these materials involves complex or unpractical manufacturing processes and often reduces the strength and electrochemical stability.

To address the main scientific issues, it is highly desirable to modify the negative grid material to meet the present day requirements. In this study, we present the feasibility and practicality of a surface treatment by CNT coating directly into the negative grid of LAB. This leads to a percolated structure even at low concentrations of CNTs, allowing highly conductive negative grid to be made. The results demonstrated the use of CNT coated negative grid as a new class of negative grid material for LAB applications.

2. Experimental section

2.1 Preparation of CNT Ink

CNTs with 40–50 nm of diameter and 5–15 μm of length purity: >99%, purchased from SRL chemical Ltd was used. CNT ink was prepared by adopting a reported method.[36] The ink prepared by dispersing 1.6 mg/mL CNT in water with 10 mg/mL sodium dodecylbenzenesulfonate (SDBS) as surfactant. After bath sonication for 5 min, the CNT dispersion was probe sonicated for 30 min to form an ink.

2.2 Cell Fabrication

The preparation method of positive and negative paste had been reported previously.[12] The plates were cured and formed as per conventional technologies.[18, 21] Here we employ conventional negative paste (0.25% Carbon black, 0.3% lignin and 0.3% barium sulfate) as the active material to make negative electrode instead of using specialized carbaneous material to demonstrate that the observed improvement in cyclability is only contributed by the CNT ink coating on the grid. The test cells were assembled with 1 negative (27mm X 25mm X 1.5mm) and 2 oversized positive plates per cell, with PVC separator. The grids were

made from lead-antimony- selenium alloy. The cells were filled with 30 mL of 1.26 sp.gr sulphuric acid (H_2SO_4). The performance of the lead- acid cells was limited by the negative plate. Figure. 1 shows a simple and overall process of CNT coated lead grid and electrode preparation process.

3. Characterization techniques

The structures were characterized by scanning electron microscopy (SEM, TESCAN). Energy-dispersive spectroscopy (EDS) was also taken on the same apparatus used for SEM. The discharge/charge voltage profiles and cyclability data were collected using with a programmable battery cycler (Bitrode) and electrochemical behavior was performed using an Auto lab electrochemical work station. The working electrode was lead alloy strip (Tab portion of the grid) geometric area of 0.70 cm^2. A platinum electrode with a large area was used as the auxiliary electrode. The reference electrode was $Hg|Hg_2SO_4|1.28\ gcm^{-3}\ H_2SO_4$. All potentials in the cyclic voltammetry experiments are reported with respect to this reference electrode. Cyclic voltammetry was performed at a scan rate of 5 mV s^{-1} in the voltage window of -0.5 to -1.3 V. The electrochemical impedance spectroscopy (EIS) was performed in the frequency range of 10 mHz -100 kHz at an AC voltage of 5 mV. EIS analysis were performed at six different potential in 1.28 sp.gr H_2SO_4 solution at room temperature

4. Result and Discussion:

As shown in Figure 2 a- b, the bare and as-prepared CNT coated lead alloy grid. The lead alloy negative grid was dipped into a black CNT ink. This dipping-and-drying cycle was repeated two times. The CNT coated grid were then placed in the vacuum oven for 10 min drying at 100 °C to remove any trapped water. After the dipping into CNT ink, the grid shows a clear color change from white to black (Figure 2b). Even at a very low concentration, CNT can serve as an efficient electron conducting network at the grid/ NAM interface.

Interestingly, during dipping process most of the CNTs were observed onto the surface of grid, but some of the CNTs were located in the grain boundary as well voids of the Pb alloy. Figure S1 shows the SEM and TEM image of pristine CNT.

4.1 FT-Raman Studies:

Raman spectroscopy provides a powerful tool for analyzing the structural characterization of carbonaceous materials. Therefore, we performed Raman measurements for with and without CNT coated lead alloy grids to further confirm the presence of carbon in the grid. As shown in Figure.3, Raman spectrum of CNT coated grid displays three prominent peaks at 1330, 1580 and 2630 cm^{-1}, mainly corresponding to the D-band (disordered structured carbon), G-band (tangential stretch mode) and 2D-band (second order or overtone of the D-band) respectively.[64] The graphitized carbon contains sp^2 hybrid bonding, which is clearly correlated with the electronic conductivity of CNT, and the disordered carbon mainly corresponds to sp^3 hybrid bonding.[65] No Raman peak of carbon appears for the bare lead grid.

4.2 SEM of with and without coated Pb alloy:

Figure 4 (a-f) shows the scanning electron micrographs comparing the microstructure of the without and with CNT coated grids. Figure 4a shows the low magnification typical structure of Pb-Sb-Se alloy. As seen in the figure 4 (b-c), grid without CNT coating indicates that a very thin grain boundary layer which is clearly visible. Meanwhile in the CNT coated grid (Figure 4 d-f) this kind of grain boundary were embraced with the CNTs, which serves a dual function as both conductive filler and also may participate in the charging process through double layer formation. This effect may be involved in our cell and the exact mechanism is unclear. Furthermore a possible mechanism could be discussed in the CV/ charge acceptance section. The typical micrograph in Figure 4 (d-f) clearly demonstrated that

CNT were well attached to the grid, which is able to provide subtle surface contact. Hence, a relatively good dispersion of the CNT on the surface of the grid is confirmed through SEM.

Moreover, it can be seen in Figure 4 (e) an intimate contact between grid and CNT, which will provide proper electronic interaction between grid and NAM interface. This can probably be attributed to the relatively better charge acceptance and conductivity. This is an indication that, CNT with high conductivity can provide an efficient electron transport pathway from current collector to skeleton structure of the NAM particles, thereby delivering enhanced capacity retention and rate capability. The morphology of CNT coated grid is slightly changed while the CNT ink dipping process. The morphological changes are attributed to presence of surfactant in the CNT ink. Interestingly, this morphology did not noticeably alter the electrochemical behavior of CNT coated grid. Apparently, there is no additional prominent peak or phase in the Raman and EDS measurement. For real applications, the grid surface is free from any residual surfactant is better; therefore, the coating method still needs to be improved in the future. In agreement with the above SEM findings, EDAX images further support the formation of uniform carbon on the CNT coated lead grid surface.

4.3 EDAX of with and without coated Pb alloy

Figure 5 (a-b) shows the EDS spectrum of with and without CNT coated grid before active mass pasting. Moreover, it is noteworthy to mention that the presence of resilient carbon signal appeared along with a major amount of lead signal, which indicating that the CNT is covered over the grid surface compared with bare grid. However, there is no study has been conducted so far on impregnating CNTAL in the negative grid of LAB.

5. Electrochemical Properties

5.1 EIS study of with and without coated Pb alloy:

A detailed impedance spectroscopy (EIS) analysis were performed at six different potential in 1.28 sp.gr H_2SO_4 solution at room temperature on with and without CNT coated grids as shown in Figure 6 (a-f). As a pretreatment, 3 cycles between -0.6 V to -1.3 V were performed at the rate of $25mVs^{-1}$. The tested electrodes were held at required potentials for 15 min before measurements. In this experiment, the electrode was subjected to potential sweep between anodic to cathodic. EIS technique has been employed to investigate the charge transfer processes occurring at electrode/solution interfaces. The semicircle is related to charge transfer resistance (Rct) and the straight line ascribes to Warburg impedance due to diffusion process. It can be observed that the diameter of the semicircle related with charge transfer resistance decreases with subsequent cathodic potential region as shown in Figure 6 (a-f). The Rct values were calculated by extrapolating the curve to a semicircle and then measuring the diameter of the semicircle.[66] At the potential -0.65V the grid surface consists of an outer $PbSO_4$ layer. At the totally discharged potential -0.65V, Figure.6 (a) shows high semicircle diameter which presumably results in the formation of a $PbSO_4$ formed over the grid surface. The Rct values do not vary much, (~ 4000 Ω) indicating that the insulating $PbSO_4$ layer covered on both the electrodes.

The impedance behavior at -0.75V, shows a different type of semicircle indicating an invariant interface between bare and CNT coated grid (Figure.6b). The decrease in the diameter of the semicircles could decrease the contact resistance and passive layer thickness by CNT coating (Rct = 157 Ω). It is considered that the CNT coating plays a role in preventing the formation of dense / irreversible hard passive layer ($PbSO_4$) reaction on the grid surface. It is obvious that there is also a sudden decrease of the Rct towards the cathodic potential window as compare with bare grid (Rct = 537 Ω). The same behavior has been observed for the potential ranges -0.85V and -0.95V. The Rct values are 8.7, 1.8 Ω for with CNT coated grid and 74, 26 Ω for without CNT coated grid. This is a clear indication of the

improvement in the conductivity of the CNT coated grid. At potentials −0.93 V, reduction of $PbSO_4$ to Pb starts. Figure. 6 (c-d) it is reasonable to expect that the conductive CNT-coating can accelerate fast electron transport between the negative grid and $PbSO_4$ layer. Moreover, this conductive CNT-coating offers additional electron pathways.

At the cathodic potential (-1.1V) CNT coated grid and bare grid exhibited an impedance of 1.42 and 14.01 Ω respectively as clearly demonstrate in Figure. 6e. This sharp decrease in Rct of CNT coated electrode upon cathodic region, which may associated with largest electrochemical active surface area due to incorporation of conducting CNT on the grid surface and complete conversion of $PbSO_4$ to Pb. Moreover, in the potential region between −0.93 V to −1.3V, a reaction of Pb^{2+} reduction to Pb proceeds. This can suggest that the CNTAL can help to decrease Rct towards cathodic process. Figure. 6 (f) shows a clear semicircle loop indicating the high Rct of bare grid (11.7 Ω). This result suggest that, at this potential (-1.3V) a tiny amount of irreversible $PbSO_4$ film is still present on the bare electrode surface. Conversely, the CNT coated electrode shows a very small semicircle loop (1.1 Ω). It is evident that the charge transfer resistance is much lower at this interface. This data exhibited that the electrode impedance continued to decreases during the cathodic sweep process, suggesting that the CNTAL gradually increased the electronic conductivity of the negative electrode.

5.2 Cyclic Voltametric (CV) study of with and without CNT coated negative grid:

In order to confirm the electrochemical behavior of with and without CNT coated grid cyclic voltammograms (Figure. 7) in the potential range from -0.5 to -1.3 V at a scan rate of 5 mV s^{-1} were recorded. The CV of these two electrode have very distinct shaped curves, and clear electrocatalytic behavior could be observed in the potential ranges, which were correlated with enhanced electron transfer rates and increased currents. In the anodic sweep, the potential region between −0.93V and −0.7 V, Pb is oxidized to $PbSO_4$. Meanwhile in the

cathodic sweep, the formed $PbSO_4$ was reduced to spongy Pb at -0.95 V to -1.11 V. The peak current value of CNT coated electrode is much higher than that of bare electrode, which means that in addition to faradaic contribution, CNT might contribute through electric double layer formation also. Moreover, the non- faradaic current for CNT coated electrode is significantly larger than that of bare electrode possibly due to the high surface area of CNT. Moreover, oxidation of Pb and reduction of $PbSO_4$ could proceeds through the CNTAL, which improves the reversibility of negative electrode. It is generally believed that CNT possesses an ideal capacitive behavior in aqueous solution due to the presence of protons which are involved in the charge storage reaction. The CNT coated grid stores energy using a non-faradaic double layer formation and also due to faradaic pseudo capacitive process such as intercalation reaction of hydrogen, which eventually improves the charge acceptance.[67] Hence this study reveals that CNTAL on grid surface may have a prominent role in improving the efficiency of LAB negative electrode performance by enabling a combination of faradaic and non -faradaic reactions. This is also one of the potential possibilities for the improved reversibility of negative electrode. The results of the CV studies are in agreement with the impedance studies. Hence, in the case of without CNT coated grid energy is stored using a conventional faradaic process of lead to lead sulfate. Our result found similarity with earlier reports by Pavlov et al. for their study on lead-carbon model electrode.[9, 68]

6. Charge/discharge cycling

In order to determine nominal capacity of the cell after its formation step, the cell was subjected to five charge/discharge cycles (20h of discharging mode, 0.05C). Subsequently, the cell was subjected to C_{10} (18 cycles) and C_5 (57 cycles) as shown in Figure. 8a. Based on the experimental results indicate low rate cycling performance has no significant change in the discharge capacity. Further, the discharge capacity (C_5) of CNT coated grid cell has been stabilized at the level of 89 $mAh.g^{-1}$ and stayed around this value with minor fluctuations up to 57 cycles. Upon increasing the cycle number the grid without CNT coating cell reflects

poor capacity retention which may be caused due to the formation of irreversible $PbSO_4$ phases during the cycling and its subsequent electrical isolation from the grid. Consequently, the poor electron transport across the grid/ NAM interlayer contribute to high charge transfer resistance and overpotential. It has been understood that the CNT coating are able to enhance the charge process and make the charge–discharge reactions more reversible.

The rate capability is compared for two cells in the discharging sequence in Figures 8b. Under all high discharge current densities, it can be seen that the discharge capacity of CNT coated electrode cell are substantially larger than that of without CNT coated electrode cell. This results show that the negative electrode with CNT coating display improved rate capability. Moreover, the discharge voltage profiles as can be seen from Figure. 8b reveal that the contact resistance at the grid / NAM particles has a strong effect on the rate performance.

Figure. 8 c-d shows the charging (C_5) voltage profiles of the cells. From Figure. 8 c, it can be seen that the charge voltages of both cells were very close to each other. Further in C_5 rate 15^{th} cycling, the potential of the uncoated grid cell is shifted by 143mV higher than that of CNT coated grid cell potential prior to 65% SoC condition as clearly seen in Figure 8d. Moreover, this behavior indicates that the hydrogen gassing potential also postponed when the CNTAL coating incorporated in the negative grid and CNT could able to increase hydrogen adsorption, storage on the surface of the CNT.[69,70] This indicates that the electrochemical reaction of Pb^{2+} reduction on the Pb surface proceeds at much lower potential at the Pb + CNT/ electrolyte interface. This behavior mainly attributed to the CNT coating reduces the polarization of the negative electrode, which accelerate the charge processes, though the discharge products are covered on the Pb grid which can easily form an insulating layer ($PbSO_4$) on the grid / active mass surfaces. In subsequent high rate cycling, the insulating layer on Pb surface would accumulate further. Hence, this also proves the

electrons flowing from the grid towards the surface of the NAM reduces some hydrogen ions to H_2 gas prior to reacting with the $PbSO_4$ layer, which will results in fast polarization as clearly revealed in Figure 8d. This may be possibly attributed to the 15^{th} charging plateau which is higher than the voltage of the third charging process in the without CNT coated grid cell.

6.1 Charge Acceptance test

In order to understand the effect of CNT coating on the lead grid, the cell has been subjected to charge acceptance test. In modern LAB operation, the high rate charging which is required in HEV applications (regenerative braking) is usually only for few seconds. In this study, the test cells were subjected to 5-s of the high rate charge with an upper voltage limit of 2.55 V.[12] Figure 9 shows the comparison of charge acceptance curves of with and without CNT coated lead electrode cell. Furthermore, CNT coated lead electrode cell has reached the higher threshold current compare with control cell. It indicates that CNT is playing a seminal role in charge processes apart from electro conductivity effects in enriching the electron transfer kinetics. Interestingly, CNTAL increases considerably the value of average double layer current in the beginning of the charge. For clear understanding, the negative electrode has a typical double-layer capacitance of 0.4–1.0 F Ah^{-1}, [52] which is not suitable to absorb short and sharp charge currents. In the present work, CNTAL contributes to increasing electrochemical active surface area as well as double layer capacitance. Apart from this, the current that flows through the negative grid initially by electric double layer reaction, which is mainly charged in the first moment of a high current pulse and completely reduce the $PbSO_4$ in the grid surface and facilitate a high rate electron transport to the skeleton structure of NAM. After a short time, the whole current flows through the faradaic reaction because very thin layer of CNTs only coated on the Pb grid surface. This is in tune with a very recent report by Pavlov et al where they showed the charging and discharging of the electric double

layer might proceeds very quickly on the electrode surface proceed mainly with first five seconds pulses.[22] It is worth mentioning that, the charge transfer resistance of the Pb/H_2SO_4 interface is high in comaprison with Pb + CNT/H_2SO_4 interface, which can facilitate the much higher current flow in this region. This correlation is supported by the impedance results demonstrated in Figure. 6.

Figure.10 presents schematic of discharging–charging of the LAB as well as tentative mechanism of electron transfer pathways in the negative electrode. The cycle life of the LAB is determined by the reversibility of the processes that proceed during discharge /charge.[71] Thus, low charge acceptance of the without CNT coated electrode, which leads to significant amount of unreduced $PbSO_4$ in the NAM as clearly confirmed in end of charge process. The first elementary process in negative electrode during charging is the dissolution (chemical reaction) of $PbSO_4$ crystals, which have direct impact on the H_2SO_4 concentration and several factors ($PbSO_4 \rightarrow Pb^{2+} + SO_4^{2-}$). Therefore, combining all of the disputes discussed above, we prudently clarify the discharging–charging process of the CNTAL electrode (Figure. 10), which can help us to understand the actual movement of the electron and reversibility of NAM. As shown in Figure. 10, since a boundless number of electrons can be obtained from the CNTAL at the beginning of charge, thus facilitates the deposition process (electrochemical reaction) much easier ($Pb^{2+} + 2e^- \rightarrow Pb$). The CNT coated grid with its high electrical conductivity leads to a higher electron density between the skeleton structure and current collector. Besides that, this model also helps us understand why the CNTAL could significantly eliminate the large polarization at early stage of high rate charge process. Moreover, CNT has a high surface area, it will lower the polarization of the negative electrodes.

7. Scanning electron microscopy of NAM after charge/discharge cycles

The morphology of the cycled NAM is revealed by SEM as shown in Figure 11. The SEM image of CNT coated grid cell NAM particles clearly reveals the typical morphology of lead and tiny amount of lead sulfate with agglomeration (Figure 11a). Moreover, NAM with small $PbSO_4$ crystals would have lower ion transferring resistance which easily allows the diffusion kinetics much easier. Hence, it is presumed that such type of morphology should enhance the electrochemical performance. From the above observations, we can conclude that the CNTAL serve as conductive media for the electron transfer process and maintains contact between the NAM particles during the discharge/charge process. Thus, the CNT coating act as a buffer zone to hamper the formation of irreversible lead sulfation during charge/discharge cycling. It was found that without CNT coated electrode cell NAM fully covered with $PbSO_4$ particles as shown in Figure. 11b. This type of $PbSO_4$ cannot, or only partially, be reconverted back to an electrochemically active form. This leads to rapid accumulation of $PbSO_4$ on the negative plate leading to early failure of the LAB.

8. Impedance measurement :

The AC impedance results obtained from the assembled test cells after 30 cycles are shown in Figure. 12. The semi circles in the Nyquist plots are depressed which may be due to the change in the resistive and capacitive components of electrode/electrolyte interface with electrode position, electrode non uniform thickness etc.[12] It is well known that a small Rct can provide logical explanation for the increased rate performance for CNT coated negative electrode in comparison with uncoated electrode at higher rates (Figure12). The data exhibited that the without CNT coated cell impedance value increases during the cycling process, suggesting that the irreversible $PbSO_4$ gradually decreased the electronic conductivity of the negative electrode.

9. Conclusion

In summary, we have demonstrated a generalized strategy for the surface modification of negative grid using CNT coating. The CNT coating allow excellent electronic conductivity and contact through Pb grid to the skeleton structure of the NAM which may also serve as a barrier against irreversible lead sulfation and capacity loss. These CNT coated grid cells have been cycled even at high rate with low capacity fading. At the same time, CNT coating helped to overcome the issue of the inherent electrical resistance associated with $Pb/PbSO_4$ redox couple. Thus, based on our experimental results, we firmly believe that CNT coating can obviously enhance the electronic conductivity of negative electrode material. This CNT coating technique offers benefits for high performance and such coating methods are becoming increasingly important in the development of LAB. A charge-discharge test revealed that at a high current rate, the grid using a CNT coating had better rate performance and its capacity faded much less, than using a bare grid. This approach offers a new way to introduce surface coating (CNT) into the negative grid in LABs and potentially become applicable for various design of the cell configuration, e.g., surface of NAM, PAM and separator materials. The extension of this new surface coating approach by various carbon/ nanostructured materials is subject of ongoing investigations.

Acknowledgement

The authors are thankful to the Council of Scientific and Industrial Research (CSIR), India for the support to carry out this work.

Supporting Information

Figure. S1: SEM and TEM image of CNT

References

1 G. Plante, C.R. *Acad. Sci. Paris,* 1860, **50,** 640-642.

2 J. Pan, Y. Sun, W. Li, J. Knight and A.Manthiram, *Nat. Commun.,* 2012, DOI: 10.1038/ncomms3178

3 J. Garche, *Phys. Chem. Chem. Phys.,* 2001, **3,** 356-367.

4 C.X. Zu, H. Li, *Energy Environ. Sci.,* 2011, **4,** 2614–2624.

5 M. Armand and J.M. Tarascon, *Nature,* 2008, **451,** 652-657.

6 Lead-based battery technologies are sustainable for the long-term, says new study, http://www.doerun.com/Portals/0/ILA%20Battery%20study%20release%20FINAL.pdf

7 K. Nakamura, M. Shiomi, K. Takahashi and M. Tsubota, *J. Power Sources,* 1996, **59,** 153-157.

8 M. Shiomi, T. Funato, K. Nakamura, K. Takahashi, and M. Tsubota, *J. Power Sources,* 1997, **64,** 147-152.

9 D. Pavlov, T. Rogachev, P. Nikolov and G. Petkova, *J. Power Sources,* 2009, **191,** 58-75.

10 M. Fernandes, J. Valenciano, F. Trinidad, and N. Munos, *J. Power Sources,* 2010, **195,** 4458-4469.

11 D. Pavlov, P. Nikolov and T. Rogachev, *J. Power Sources,* 2010, **195,** 4435-4443.

12 M. Saravanan, M. Ganesan and S. Ambalavanan, *J. Power Sources,* 2014, **251,** 20-29

13 D.P. Boden, D.V. Loosemore, M.A. Spense and T.D. Wojcinski, *J. Power Sources,* 2010, **195** 4470-4493.

14 D. Pavlov, P. Nikolov and T. Rogachev, *J. Power Sources,* 2011, **196,** 5155-5167.

15 R. Shapira, G. D. Nessim, T. Zimrin, and D. Aurbach*, Energy Environ. Sci.,* 2013, **6,** 587-594.

16 B. Hong, L. Jiang, H. Xue, F. Liu, M. Jia, J. Li and Y. Liu, *J. Power Sources,* 2014, **270,** 332-341.

17 L. Zhao, W. Zhou, Y. Shaob and D. Wang, *RSC Adv.,* 2014, **4,** 44152- 44157.

18 S. M. Kumar, S. Ambalavanan and S. Mayavan, *RSC Adv.,* 2014, **4,** 36517- 36521.

19 S. Logeshkumar and R. Manoharan, *Electrochim. Acta,* 2014, **144,** 147–153.

20 B. Hong, X. Yu, L. Jiang, H. Xue F. Liu, Jie Li and Y. Liu, *RSC Adv.,* 2014, **4,** 33574-33577

21 M.Saravanan, P.Sennu, M.Ganesan and S.Ambalavanan, *J. Electrochem. Soc.,* 2013, **160,** A70-A76.

22 D. Pavlov and P. Nikolov, *J. Power Sources,* 2013, **242,** 380-399.

23 S. Lee and E.S. Oh. *J. Power Sources,* 2013, **244,** 721-725.

24 Z. Zhang, Z. Zhang, X. Wang, J. Li and Y. Lai, *J Appl. Electrochem.,* 2014, **44,** 607–611.

25 C. Zu, Y.-S. Su, Y. Fu and A. Manthiram, *Phys. Chem. Chem. Phys.,* 2013, **15,** 2291-2297.

26 Y.S. Su, and A. Manthiram, *Nat. Commun., 2013,* DOI: 10.1038/ncomms2163.

27 Y.S. Su and A. Manthiram, *Chem. Commun.,* 2012, **48,** 8817–8819.

28 S.H. Chung and A. Manthiram, *Chem. Commun.,* 2014, **50,** 4184-4187.

29 X. Yu and A. Manthiram, *Chem. ElectroChem.,* 2014, **1,** 1275 – 1280.

30 Z. Zhang, Z. Zhanga, K. Zhanga, X. Yanga and Q. Lia, *RSC Adv.,*2014, **4,** 15489-15492.

31 F. Qin, K. Zhang, J. Fang, Y. Lai, Q. Li, Z. Zhang and J. Li, *New J. Chem.*, 2014, **38,** 4549-4554.

32 X. Wang, Z. Wang and L, Chen, *J of power sources,* 2013, **242,** 65-69.

33 G. Yu, L. Hu, N. Liu, H. Wang, M. Vosgueritchian, Y. Yang, Y. Cui, and Z. Bao, *Nano Lett.* 2011, **11,** 4438–4442.

34 D.Y. Cho, K. Eun, S.H. Choa, H.K. Kim, Carbon, 2 0 1 4, **6 6,** 5 3 0 –5 3 8.

35 H.T. Jeonga, B. C. Kimb, R. Gorkina, M. J. Higginsa and G. G. Wallacea, *Electrochim. Acta,* 2014, **137,** 372–380.

36 L.Hu, M. Pasta, F. L. Mantia, L. Cui, S. Jeong, H. D. Deshazer, J. W. Choi, S. M. Han, and Y. Cui, *Nano Lett.* 2010, ***10*****,** 708-714.

37 H.Y. Tsai, C.C.Wub, C.Y. Leec and E. P. Shiha, *J. of power sources,* 2009, **194,** 199–205.

38 S. G. Hashmi , J. Halme, Y. Ma, T. Saukkonen, and P. Lund, *Adv. Mater. Interfaces,* 2014, *1,* 1300055- 1300060.

39 W.w, Liu, X.b. Yan, J.w. Lang, C. Penga and Q.j. Xue, *J. Mater. Chem.,* 2012, **22,** 17245-17253.

40 J. Hou, Z. Liu, S. Yang, and Y. Zhou, *J. of power sources,* 2014, **258,** 204 – 209.

41 D. Pavlov, *J. of power sources,* 1995, **53** 9-21.

42 R.J. Ball, R. Kurian, R. Evans and R. Stevens, *J. of power sources,* 2002, 111, 23–38.

43 A.F. Hollenkamp, K.K. Constanti, M.J. Koop, L. Apiiteanu, M. Calabek and K. Micka *J. of power sources,* 1994, **48**, 195-215.

44 S. Zhong, H.K. Liu, S.X. Dou and M. S.Kazaco, *J. of power sources,* 1996, **59,** 123-129.

45 I. Kurisawa, M. Shiomi, S. Ohsumi, M. Iwata and M. Tsubota, *J. of power sources,* 2001, **95,** 125-129.

46 M. Cruz, L. Hernan, J. Morales and L. Sanchez, *J. of power sources,* 2002, **108,** 35–40.

47 G. Barkleit, A. Grahl, M. Maccagni, M. Olper, P. Scharf, R. Wagner and H. Warlimont, *J. of power sources,* 1999, **78**, 73–78.

48 K. Ji, C. Xu, H. Zhao and Z. Dai, *J. of power sources,* 2014, **248,** 307-316.

49 R. Demarco and A. Rochliadi, and J. Jones, *J. of Applied electrochemistry,* 2001, **31,** 953-959.

50 K. Yamada., K.i. Maeda, K. Sasaki and T. Hirasawa, *J. of power sources,* 2005, **144,** 352–357.

51 W.H. Kao, S. L. Haberichter, and K. R. Bullock, *J. Electrochem. Soc.,* 1992, **139,** L105-107.

52 P. T. Moseley, D.A.J. Rand and B. Monahov, *J. of power sources,* 2012, **219,** 75 -79.

53 L.T. Lam., N.P. Haigh, C.G. Phyland and T.D. Huynh, *J. of power sources,* 2005, **144,** 552–559.

54 V.Iliev and D. Pavlov, *J. of Applied electrochemistry,* 1985, **15,** 39-52.

55 D. Pavlov, S, Ignatova, *J. of Applied electrochemistry,* 1987, **17,** 715-723.

56 D. Pavlov, and V.Iliev, *J. of power sources,* 1982, **7,** 153 – 164.

57 M. Calabek, K. Micka, P. Baca and P. Krivak, *J. of power sources,* 2000, **85,** 145–148.

58 P. Krivak, P. Baca, M. Calabek, K. Micka, and P. Kral, *J. of power sources,* 2006, **154,** 518–522.

59 B. Hariprakash and S.A. Gaffoor, *J. of power sources,* 2007, **173,** 565–569.

60 A. Czerwinski, S. Obrebowski and Z. Rogulski, *J. of power sources,* 2012, **198,** 378– 382.

61 Y. Chen, B.Z. Chen, L.W. Ma and Y. Yuan, *Electrochem. Commun.,* 2008, **10,** 1064–1066.

62 Y.-I. Jang, N. J. Dudney, T. N. Tiegs and J. W. Klett, *J. of power sources,* 2006, **161,** 1392–1399.

63 S.K. Martha, B. Hariprakash, S.A. Gaffoor and A.K. SHUKLA, *J. of Applied electrochemistry,* 2006, 36, 711–722.

64 M. S. Dresselhaus, A. Jorio, M. Hofmann, G. Dresselhaus, and R. Saito, *Nano Lett.*, 2010, **10,** 751–758.

65 C. S. Rout, A. Kumar, T. S. Fisher, U. K. Gautam, Y. Bandoc and D. Golberg, *RSC Adv.,* 2012, **2,** 8250–8253

66 S. C. Raghu a, M. Ulaganathan, T. M. Lim and M. S. Kazacos, *J. of power sources,* 2013, **238,** 103-108.

67 M. Saravanan, M. Ganesan, and S. Ambalavanan, *J. Electrochem. Soc.,* 2012, **159,** A452-A458.

68 D. Pavlov, P. Nikolov, and T. Rogachev, *J. of power sources,* 2010, **195,** 4444-4457.

69 S. W. Swogger , P. Everill, D.P. Dubey and N. Sugumaran, *J. of power sources,* 2014, **261,** 55- 63.

70 N. Sugumaran, P. Everill, S. W. Swogger and D.P. Dubey, *J. of power sources*, 2015, **279,** 281-293.

71 D. Pavlov and P. Nikolov, *J. Electrochem. Soc.,* 2012, **159,** A1215 - A1225.

Figure Caption:

Figure1: Schematic represenation of overall process of CNT coated lead grid and electrode preparation process

Figure 2: (a-b) shows a photograph of a representative bare and CNT coated lead alloy grid.

Figure 3: Raman spectra of (a) Pb grid and (b) CNT coated Pb grid, using 632.8 nm diode laser excitation.

Figure 4: SEM images of (a-c) without and (d-f) with CNT coated lead alloy grid

Figure 5: EDX spectroscopy of (a) Without CNT coating, (b) With CNT coated negative grids.

Figure 6: Nyquist spectra obtained on with and without CNT coated negative electrode at various potentials.

Figure 7: Cyclic voltammograms of the with and without CNT coated negative grid.

Figure 8: (a) Cycling performance, (b) Discharge curves at different current densities, (c) charge curves at 3^{rd} cycle and (d) 15^{th} cycle (C_5) rate.

Figure 9 : Charge acceptance curves of with and witout CNT coated negative electrode cells

Figure 10: Schematic showing the discharge – charge reaction in LAB and a tentative mechanism for the electron flow / pathways in the negative electrode.

Figure 11: SEM images of with (a) and (b) without CNT coated grid cell NAM

Figure 12. Electrochemical impedance spectra of the lead –acid cell. (after 30 cycles)

FIGURE 1

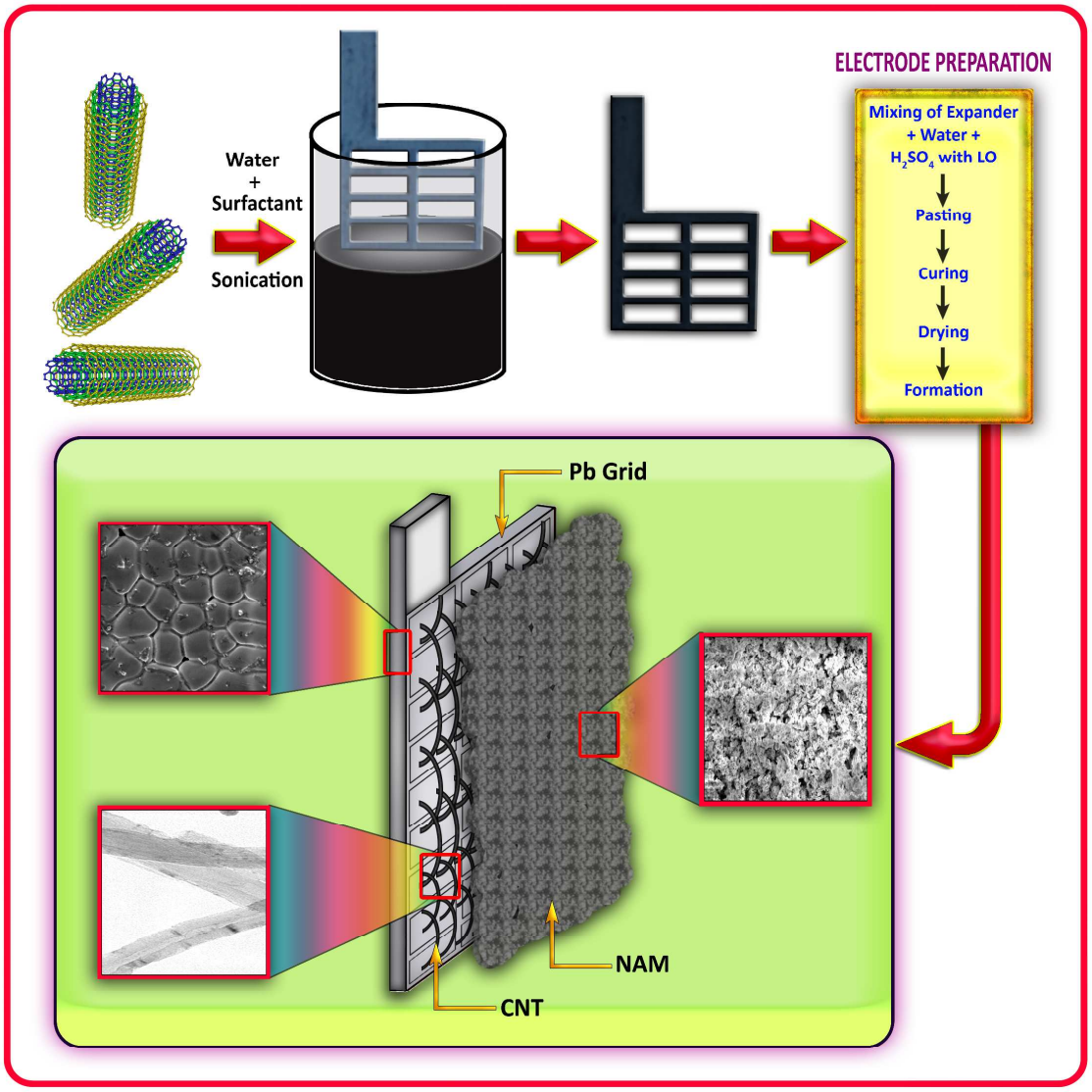

FIGURE 2

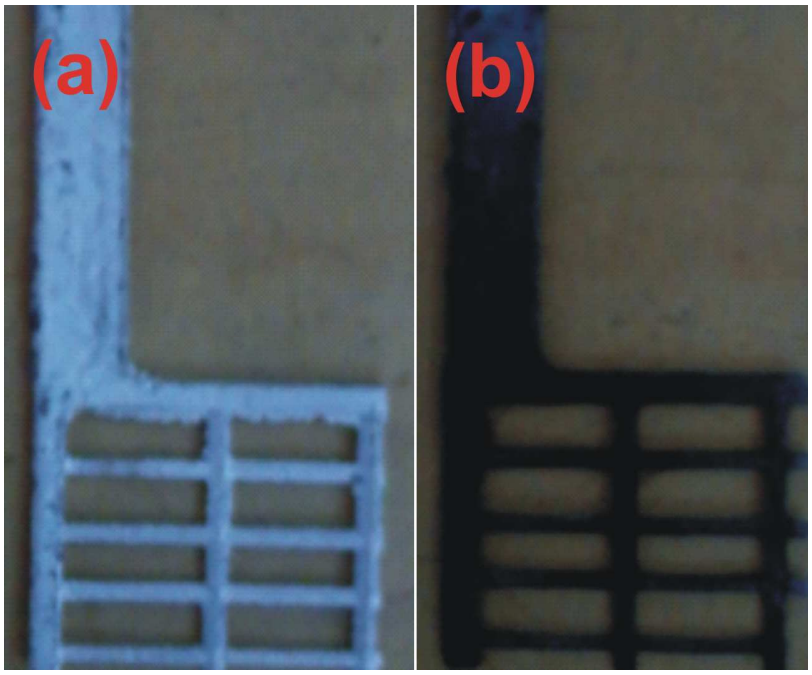

FIGURE 3

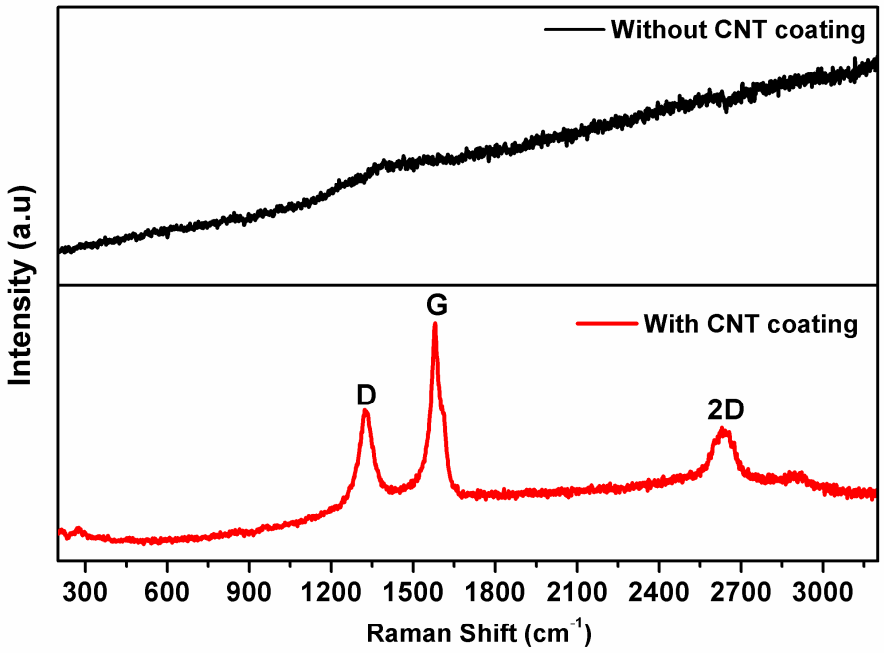

FIGURE 4

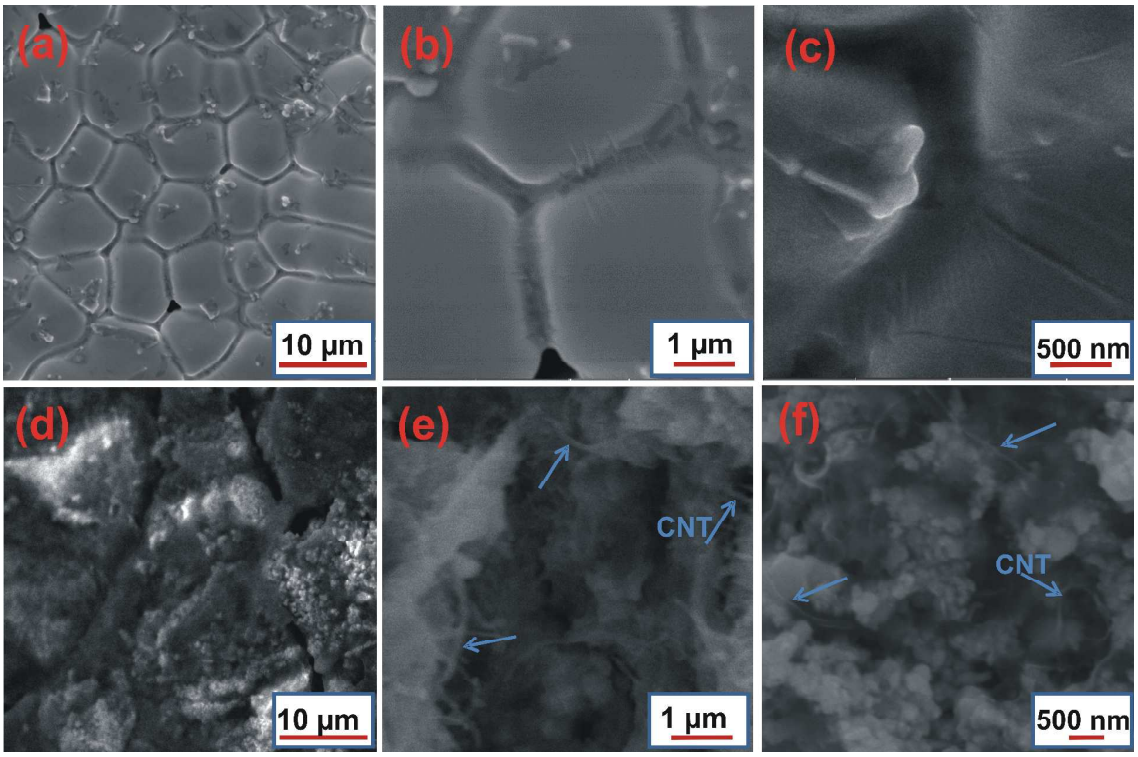

FIGURE 5

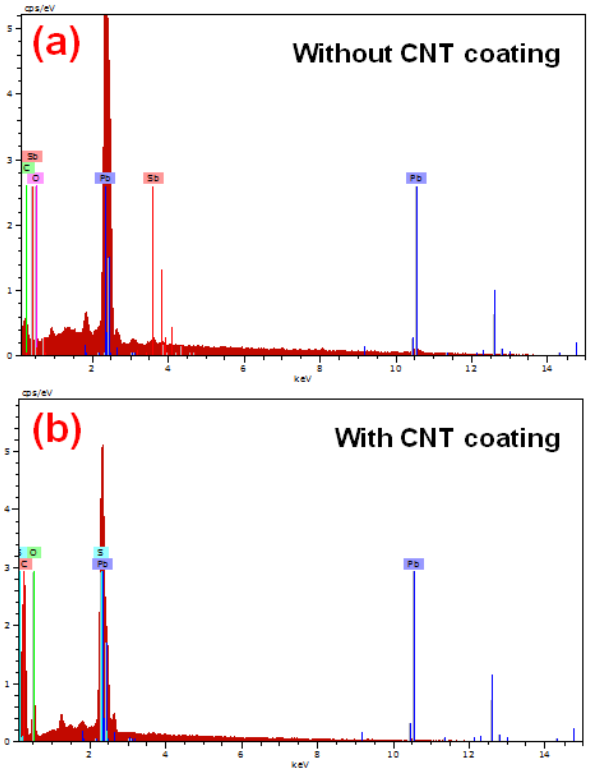

FIGURE 6

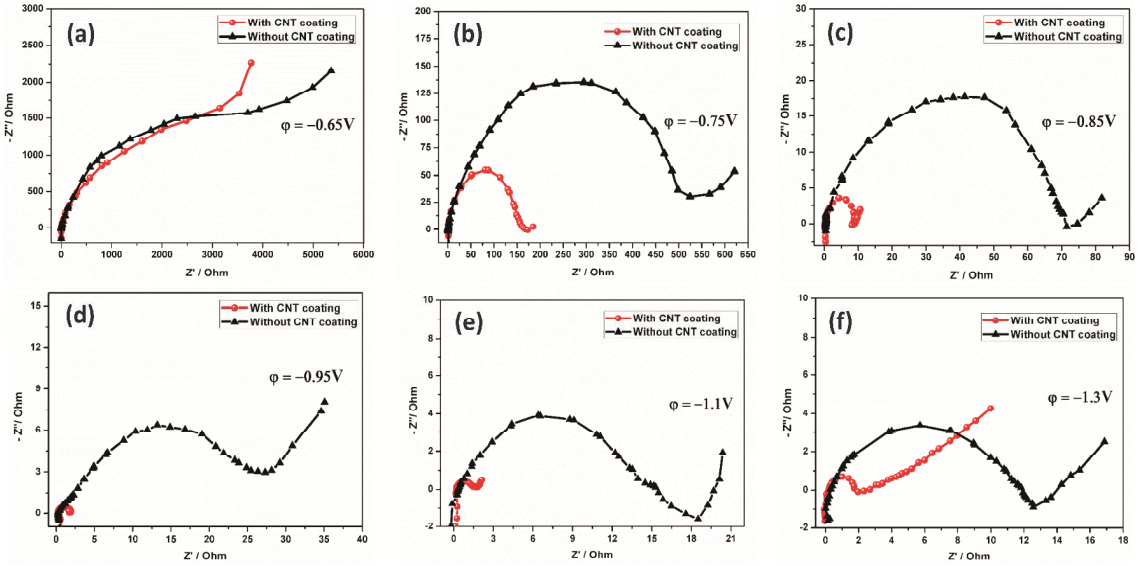

FIGURE 7

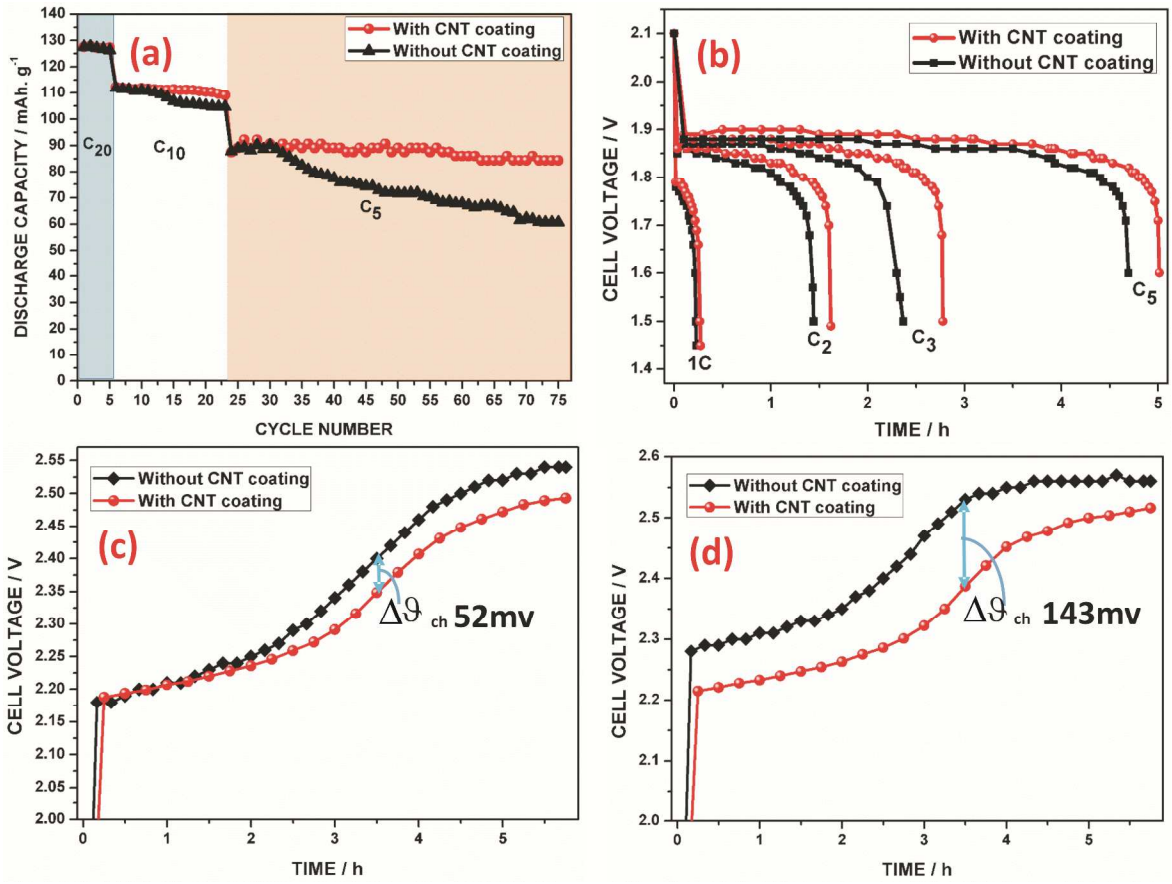

FIGURE 8

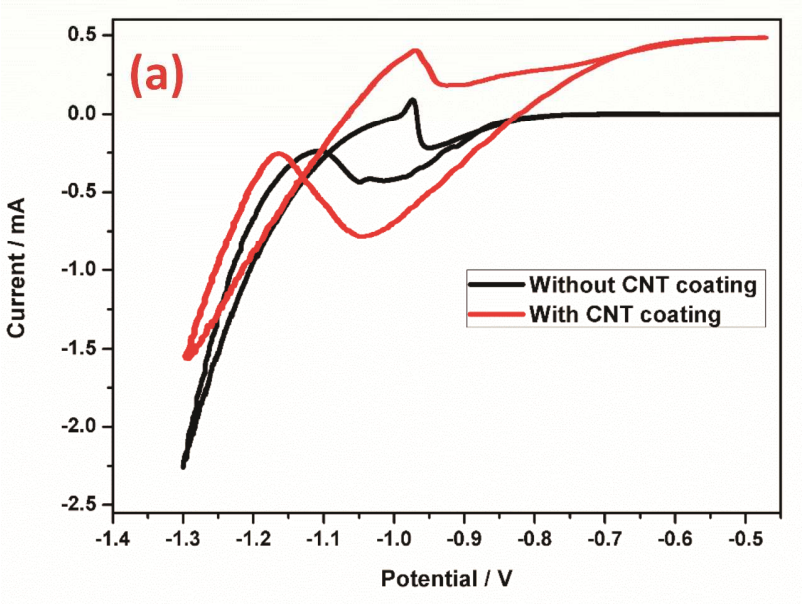

FIGURE 9

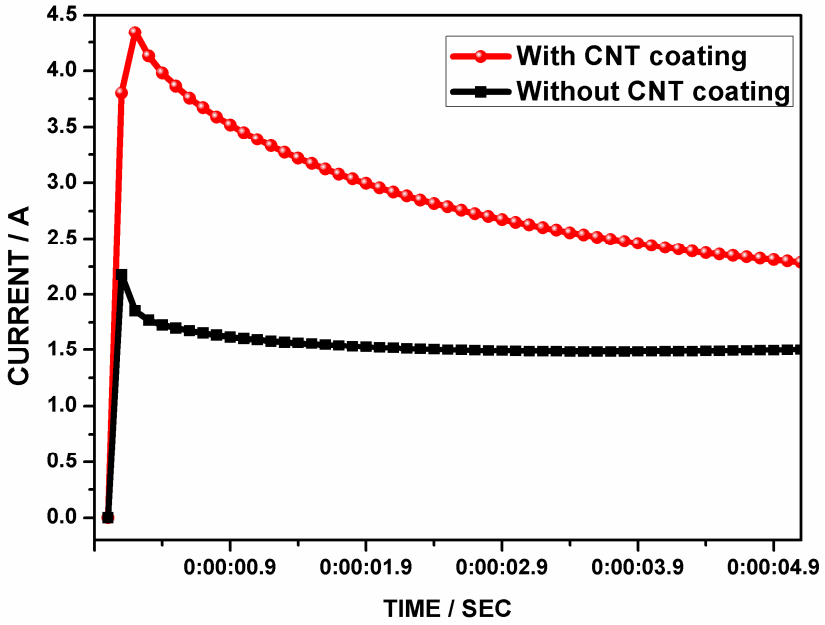

FIGURE 10

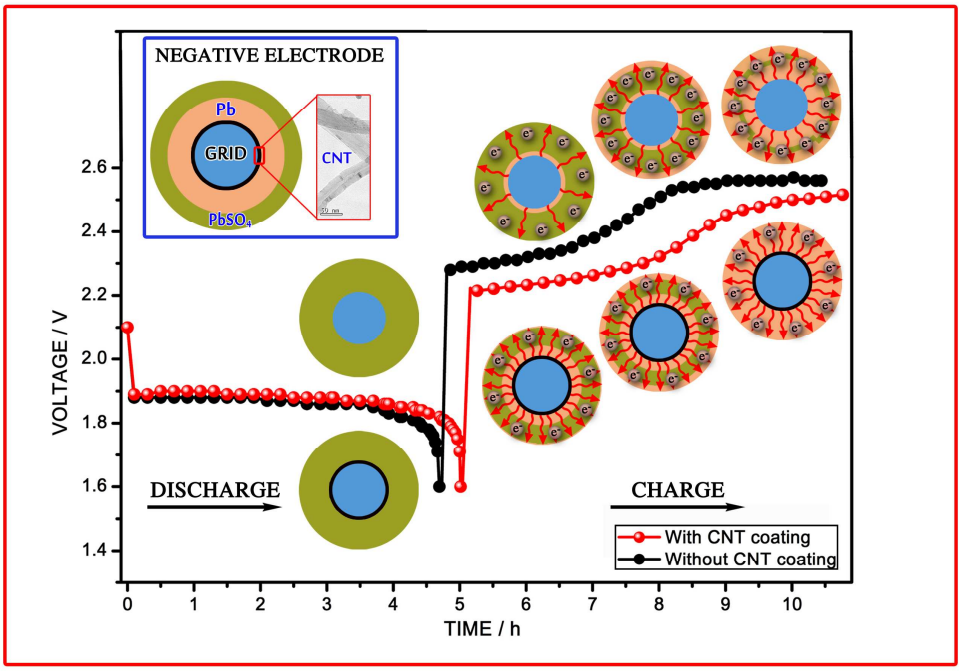

FIGURE 11

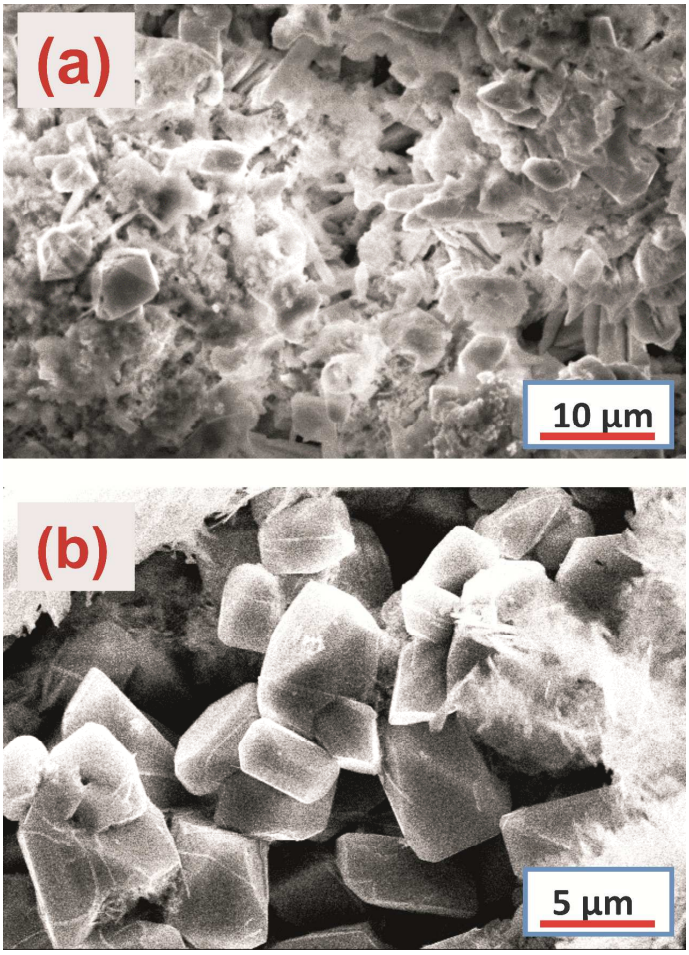

FIGURE 12